OPEN ACCESS
IOP Publishing | ISECAEP
Journal of Reliability Science and Engineering
J. Reliab. Sci. Eng. **1** (2025) 025302 (17pp)
https://doi.org/10.1088/3050-2454/add01a

Physical model-driven performance degradation analysis of planetary gearboxes

Hongrui Cao[1,2], **Chaohu Wei**[1,2] **and Xuefeng Chen**[1,2,*]

[1] National Key Lab of Aerospace Power System and Plasma Technology, Xi'an Jiaotong University, Xi'an 710049, People's Republic of China
[2] School of Mechanical Engineering, Xi'an Jiaotong University, Xi'an 710049, People's Republic of China

E-mail: chenxf@xjtu.edu.cn

Received 12 February 2025, revised 18 March 2025
Accepted for publication 7 April 2025
Published 13 June 2025

Abstract

Planetary gearboxes are extensively used in mechanical equipment, such as automotive and wind turbines, and the performance degradation analysis is essential for prognostics health management of the equipment. However, traditional methods heavily rely on lifecycle monitoring data which is expensive and difficult to obtain in practice. To address these issues, this study proposes a physical model-driven performance degradation analysis method of planetary gearboxes. Firstly, a dynamic model of a typical planetary gearbox is developed, and then verified with experiments. With the dynamic model, dynamic responses of the planetary gearbox that are difficult to measure are simulated. Secondly, the progression of damage to the inner ring of the bearing is incorporated into the dynamic model as time-varying excitation forces, resulting in a new dynamic model that incorporates bearing degradation. The dynamic responses of the planetary gearbox during the initial degradation process are calculated. Finally, by extracting degradation information from multiple measurement points using the dynamic model and fusing data from eight various sensors, a novel real-time degradation indicator based on vibration velocity signals is proposed for gearbox condition monitoring. The results show the lifetime degradation of planetary gearboxes, offering new insights into gearbox state monitoring and failure prediction.

Keywords: dynamic model, planetary gearbox, performance degradation, vibration analysis

1. Introduction

Planetary gearboxes are widely used in aerospace, automotive and other large transmission machinery [1] with complex nonlinear dynamic characteristics. Unlike simple parallel-axis gear transmissions or other conventional transmission forms, planetary gear systems are required to handle significantly larger loads and higher transmission ratios [2]. Even with optimal design and manufacturing processes, degradation phenomena such as gear cracks [3] and bearing failures [4] may still occur over time. A comprehensive understanding of the degradation mechanisms of key components, such as gears and bearings, within planetary gearboxes is essential for enabling predictive maintenance strategies.

Data-driven and deep learning methodologies have been extensively used to analyze the degradation of bearings and other gearbox components. However, the effectiveness of deep learning models is primarily contingent upon the quantity and

* Author to whom any correspondence should be addressed.

Original content from this work may be used under the terms of the Creative Commons Attribution 4.0 licence. Any further distribution of this work must maintain attribution to the author(s) and the title of the work, journal citation and DOI.

© 2025 The Author(s). Published by IOP Publishing Ltd on behalf of the Institute of Systems Engineering, China Academy of Engineering Physics

quality of degraded data available for training, which significantly influences the accuracy and reliability of the learning outcomes [5]. Wang *et al* [6] established a dataset of bearing life called XJTU-SY data for different damage modes using bearing life testing equipment and proposed a new method for predicting bearing life. Based on this dataset, Qin *et al* [7] established a bearing model that can reveal the full life operating status of the bearing, Li *et al* [8] proposed a dynamic normalized health indicator and used it to predict the remaining useful life of high-speed bearing in wind turbine drivetrain. Ni *et al* [9] proposed a novel health indicator and gated recurrent unit network to real-time characterize the operating status of bearings, and the new method was also applied and validated by XJTU-SY data. In addition to this set of data, there are also a few experimental data that are often used in the degradation analysis of bearings. Mao *et al* [10] proposed a deep feature representation and transfer learning method to study the performance degradation of rolling bearings based on the prognostics health management Challenging 2012 data set. On the basis of the same data set, Zhu *et al* [11] developed a new data-driven transferable remaining useful life prediction approach under different working conditions, Deng *et al* [12] proposed a new transfer learning framework to figure out the degradation of rolling bearings. It can be observed that most studies on degradation are limited to a small number of degradation test data, primarily due to the high cost of degradation experiments and the difficulty in achieving ideal experimental results. The data limitation hinders the development of generalized degradation analysis methods that can be universally applied.

In the degradation research of planetary gearboxes, many scholars also rely on the analysis of experimental data and signal processing methods. Ma *et al* [13] proposed two indicators based on experimental vibration signals to quantify the process of tooth root crack propagation. Ni *et al* [14] proposed a new improved kurtogram and applicated to planetary gearbox degradation feature analysis. Pan *et al* [15] assessed the performance degradation of a wind turbine gearbox based on multi-sensor data fusion. Sun *et al* [16] created an online degradation feature extraction technique for shore bridge gearbox based on morphological fractal dimension and sliding window Weibull fitting. Ma *et al* [17] assessed the gearbox degradation based on a sparse representation feature and Euclidean distance method. Due to the scarcity of experimental data, some scholars have used probabilistic methods to study the degradation of planetary gearboxes. Qiao *et al* [18] proposed a new degradation feature extraction method of planetary gearbox based on alpha stable distribution. Chen *et al* [19] proposed a generalized degradation tendency tracking strategy for gearbox remaining useful life prediction. Caso *et al* [20] finished an experimental study of acoustic emissions from active surface degradation in planetary gears. It is easy to see that the degradation data of the gearbox is very rare and the fatigue life test of gear transmission system is very time-consuming and costly. In this context, simulation models offer a promising solution to mitigate the issue of insufficient experimental data, enabling the derivation of degradation laws based on the inherent characteristics of mechanical systems.

Some scholars have used model-driven methods to study the performance degradation of simple components such as bearings. Luo *et al* [21] evaluated the defect area of a rolling element bearing based on physical modeling and instantaneous vibration energy investigation. Shi *et al* [22] proposed a novel model for dynamical updating and real-time mapping of local defect extension in rolling bearings. One important role of this dynamic model is to achieve the prediction of bearing life. Both Ma *et al* [23] and Song *et al* [24] established dynamic models of bearings that can operate under variable working conditions, and based on their models, diagnosis can be carried out with a small amount of experimental data. Zhao *et al* [25] used ADAMS to establish a dynamic model of the bearing, and used CycleGAN network to correct the simulation data, ultimately obtaining twin data that can meet the requirements of state monitoring. Based on the integration of transfer learning and dynamic simulation, Liu *et al* [26] proposed a data-model joint-driven intelligent diagnostic framework for bearings. When the signals of bearings and gears are fused together, it becomes more difficult to study the degradation of bearings. Chen *et al* [27] has established a dynamic model of the helicopter tail transmission system and is able to predict bearing failures in the transmission system. Ishihara *et al* [28] established a dynamic model of wind turbine and has achieved the prediction of the service life of the main bearing. We can find that research on the degradation of a single bearing based on physical models has been very in-depth. But the planetary gear transmission system is a very complex mechanical structure.

Given the complexity of the dynamic behavior inherent in planetary gearboxes, numerous researchers have developed simulation models to study their performance degradation mechanism. Zhu *et al* [29] established an electromechanical coupling model of the planetary gear transmission system based on ADAMS, and the model was able to accurately simulate the dynamic response when both the sun gear and the planetary gear fail simultaneously. Yang *et al* [30] established a dynamic model of planetary gear transmission system containing different types of gear faults, revealing the influence of different fault modes on the dynamic response of planetary gearbox. Wei *et al* [31] developed a dynamic model of a planetary gearbox with bearing faults based on SIMPACK, and analyzed the transmission process of vibration signals inside the gearbox. After completing the establishment of the dynamic model, the next step is to use the dynamic models to study the fault mechanism and degradation mechanism of gearboxes. Moghadam and Nejad [32] proposed an online condition monitoring method of floating wind turbines drivetrain by means of a dynamic model. Combining simulation data with experimental data is a very good means of studying gearbox degradation. Yu *et al* [33] presented a gearbox fault diagnosis framework based on a fusion model of virtual physical model and data-driven method. Deng *et al* [34] proposed a life prediction model considering the interaction of factors such as dynamic load, grain size, initial crack length, residual stress, slip band length and width. Compared to experiments, studying the degradation of gear transmission systems based

on dynamic models can save a lot of time and money. Feng *et al* [35] established a dynamic model of a pair of spur gears that can evaluate the wear process of gears. Kumar *et al* [36] established a dynamic model of a single stage gearbox and calculated the performance degradation process. Currently, dynamic modeling and fault simulation techniques for planetary gearboxes have become highly advanced and are widely utilized in fault diagnosis. However, research on the degradation mechanisms based on the dynamic models of planetary gearboxes remains limited. Model-driven approaches for performance degradation analysis in planetary gearboxes could serve as a valuable complement to degradation analysis based on experimental data.

The above literature indicates that the majority of current research on the degradation state assessment of planetary gearboxes primarily relies on signal processing and machine learning techniques. However, these approaches are limited by the challenges of obtaining real-world degradation data from planetary gearbox testing. To date, studies utilizing dynamic models for degradation analysis have predominantly focused on simpler components, such as bearings, while the degradation of planetary gear transmission systems as a whole remains largely unexplored. In this paper, firstly, a dynamic model of the planetary gearbox was developed using the multi-body dynamics method, and its accuracy was validated through experimental testing. This model facilitated a comprehensive understanding of the dynamic characteristics of the planetary gearbox that are challenging to detect experimentally, including time-varying meshing stiffness (TVMS), dynamic transmission error (DTE), and bearing support forces during operation. Secondly, a distinct fault excitation forces incorporating time-varying degradation characteristics of the bearing, were introduced into the established planetary gearbox dynamic model. This integration resulted in a novel and refined dynamic model that encapsulates the time-varying degradation behavior of the bearings. Subsequently, a new degradation index for the planetary gearbox based on vibration velocity was proposed. This index synthesizes vibration signals obtained from sensors placed at various locations to quantitatively describe the evolution of the gearbox's dynamic response as the bearings degrade. This approach offers valuable insights for predictive maintenance of planetary gearboxes using dynamic simulation technology.

2. Dynamics modeling of planetary gearbox

A comprehensive understanding of the dynamic characteristics of planetary gearboxes cannot be solely achieved through experimental methods or dynamic simulations alone. Dynamic modeling techniques are capable of incorporating nonlinear factors, such as dynamic mesh stiffness and DTE, which arise during gear interactions. These models can also simulate critical physical quantities such as gear meshing forces and bearing support forces that are difficult to measure with current sensing technologies. However, due to limitations in computational power, dynamic models often require simplifications of real-world systems, which may not fully capture boundary conditions such as bolt connections and lubrication effects. As a result, only a limited set of physical quantities, such as shaft rotational speed and gearbox casing vibrations, can be simultaneously simulated and experimentally validated. Furthermore, the rotational speeds of internal shafts and the vibrations of rotating components remain challenging to quantify experimentally. Therefore, an integrated approach that combines dynamic modeling with empirical observations is essential to achieving a more complete and accurate understanding of the dynamic characteristics of planetary gearboxes. Figure 1 illustrates the relationship between the dynamic model and the physical entity of a planetary gearbox. It is evident that dynamic models and physical entities complement each other, collectively generating critical data within the framework.

2.1. Dynamics modeling

2.1.1. Multi-body dynamic theory. Due to its high computational speed and consideration of multiple degrees of freedom, multi-body dynamics models are widely used in the dynamic modeling and vibration simulation analysis of planetary gearboxes. In this paper, the dynamic model of a planetary gearbox is presented by SIMPACK software and the motion relationships among different parts can be expressed as equation (1) [37]:

$$\begin{cases} \dot{z}_p = z_v \\ M\dot{z}_v - \boldsymbol{G}^T\lambda = h(z_p, z_v, t) \\ g(z_p, t) = 0 \end{cases} \tag{1}$$

where z_p denotes the redundant position variables and z_v contains the redundant velocity variables. The dot above a symbol means the derivative for time t. The matrix $\boldsymbol{M}$ represents the mass and inertial matrix, and $\boldsymbol{h}(z_p, z_v, t)$ is the vector of generalized applied forces. The matrix $\boldsymbol{G}$ represents the constraint modes of motion and λ is the Lagrange multiplier associated with the constraints. Vector $\boldsymbol{g}$ describes the constraint equations on the position level. The dynamic responses of any component in the MBD (Multi-body dynamics) model of planetary can be obtained by the equations above.

The calculation method for TVMS of gears $k(t)$ is as equation (2):

$$k(t) = k_{\max}\left\{1 - \left(1 - \frac{k_{\min}}{k_{\max}}\right)\left(\frac{s(t)}{s_{\max}}\right)^2\right\}. \tag{2}$$

Here $k_{\max}$ is the normal contact stiffness at the pitch point, $k_{\min}$ is the effective tooth pair contact stiffness acting at a tooth height equal to the normal module counting from the pitch circle, $s(t)$ is the distance between the meshing point and the pitch point at time t, and $s_{\max}$ is the maximum value between the meshing point and the pitch point.

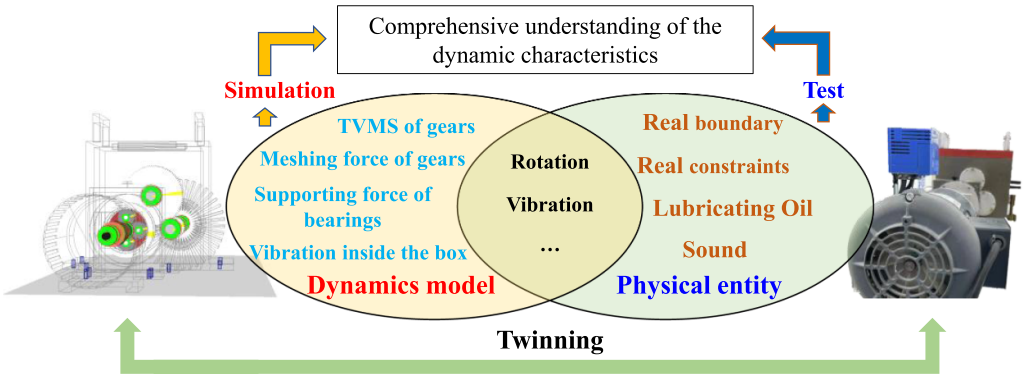


Figure 1. The relationship between dynamics model and physical entity.

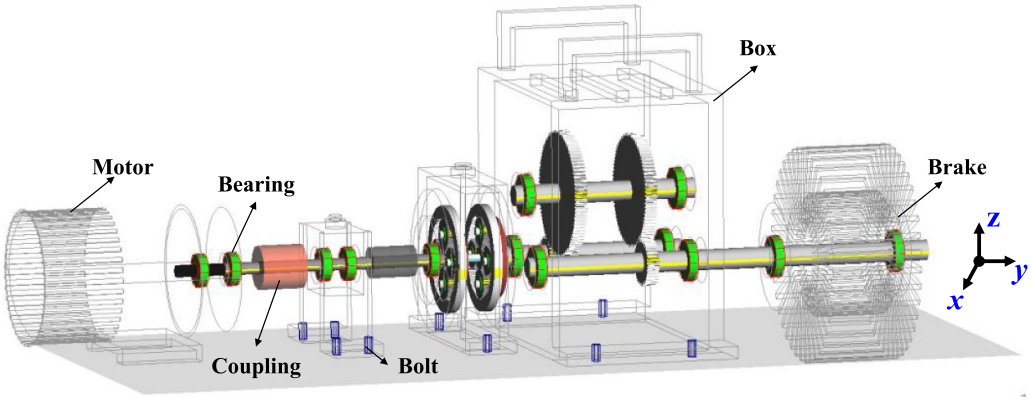


Figure 2. The dynamic model of the planetary gearbox drivetrain.

The DTE (t) of gears is also considered while modeling as equation (3):

$$DTE(t) = R_{b1}\varphi_1(t) + R_{b2}\varphi_2(t) \tag{3}$$

where R_{b1} and R_{b2} are the base radiuses of two gears meshing with each other, $\varphi_1(t)$ is the rotating angle of gear 1, and $\varphi_2(t)$ is that of gear 2.

Different bearing models can be embedded into MBD models, but considering the fast calculation characteristics, the bearings are simplified. The simplified bearing model considers motions at four directions: axial translation, radial translation, torsional, and tilting as equation (4). Here k_a, k_r, k_α and k_ψ are stiffness coefficients in axial, radial, torsional, and tilting direction accordingly, d_a, d_r, d_α and d_ψ are damping values of the four directions respectively. Forces and moments in the four directions between the shaft and the bearing block are defined as F_a, F_r, T_α and T_ψ. In this equation, a and r are the axial and radial distance, α and ψ are the torsional and tilting angle of the shaft relative to the housing

$$\begin{bmatrix} F_a \\ F_r \\ T_\alpha \\ T_\psi \end{bmatrix} = \begin{bmatrix} k_a \cdot a + d_a \cdot \dot{a} \\ k_r \cdot r + d_r \cdot \dot{r} \\ k_\alpha \cdot \alpha + d_\alpha \cdot \dot{\alpha} \\ k_\psi \cdot \psi + d_\psi \cdot \dot{\psi} \end{bmatrix}. \tag{4}$$

In order to maintain a stable output speed, the input power and load of the planetary gearbox need to satisfy a certain proportional relationship. The relationship between the input torque T_{in} and the load damping d_{out} is shown as equation (5). Here T_{in} means the input torque, ζ means the transmission ratio of the drivetrain system, n_{out} means the rotation speed of output shaft and d_{out} means the damping acting at the output shaft.

$$T_{\text{in}} = \zeta \cdot n_{\text{out}} \cdot d_{\text{out}}. \tag{5}$$

2.1.2. Dynamics model of a typical planetary gearbox. Figure 2 illustrates the dynamic model of the planetary gearbox drivetrain system, developed using SIMPACK software, alongside the corresponding physical entity. While modeling, it is assumed that all moving components are rigid bodies with uniformly distributed mass. The actual dimensions of the test rig are measured, and then, considering parameters such as the geometric shape, material density, and other characteristics of components like the housing and gears, each moving part is developed. The dynamic characteristics of these components are defined by considering the actual constraint relationships. It should be noted that this model only accounts for mechanical motion, and environmental factors such as lubrication and temperature effects on the test rig are neglected. To accurately replicate the dynamic characteristics of the test bench, the

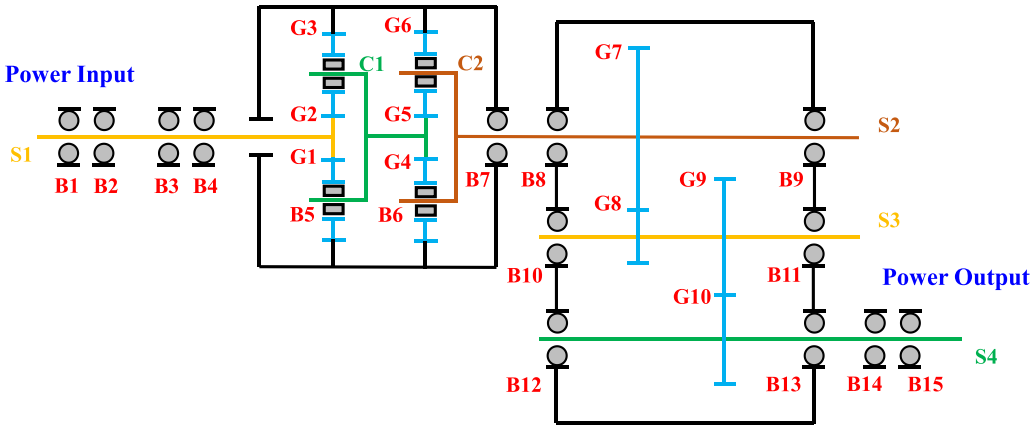


Figure 3. The kinematic scheme of drivetrain system.

inertial loads of key components, namely the housing, motor, and brake were incorporated into the modeling process. This allows the model to operate under conditions that are closer to reality.

In the original system configuration, the shaft is supported by bearings within the housing; however, in the dynamic model, this bearing support is simplified to a 2×2 stiffness-damping matrix. In this test rig, almost all the bearings use the same model, and thus their stiffness and damping coefficients are based on the same set of data: radial support stiffness of 1×10^9 N m^{-1}, radial damping of 1×10^6 Nm s^{-1}, axial support stiffness of 1×10^8 N m^{-1}, and axial damping of 1×10^5 Nm s^{-1}. Similarly, the bolts connecting the housing to the base are represented using a stiffness-damping matrix. Considering that the vibration in the y-direction is relatively small, the connection stiffness in the x and z directions is set to be higher than that in the y-direction. The connection stiffness for each bolt in the x and z directions is set to 1×10^7 N m^{-1}, while in the y-direction, it is set to 1×10^6 N m^{-1}. The damping values in all three directions are set to one-thousandth of the stiffness values in their respective directions. In the modeling process, TVMS, DTE, friction, damping, and the influence of couplings on rotor mass were all considered. It is important to note that the moving components, such as the shaft, housing, and gears, in the dynamic model possess six degrees of freedom relative to the inertial reference frame.

In the operational scenario of the drivetrain system, power is input from the motor side, while the load is applied at the brake end. This same operational configuration is mirrored in the dynamic model, the input torque is 8.83 Nm and the load damping is 100 Nms rad^{-1}, with the final input speed maintained at 1200 r min^{-1}.

Figure 3 presents the transmission diagram of the drivetrain system. Within the dynamic model, there are four shafts, labeled sequentially as S1, S2, S3, and S4. Power is input through S1 and is transmitted to S4 via two planetary gear stages and two pairs of meshing spur gears. The dynamic model incorporates a total of 15 bearings, each characterized by distinct parameters and labeled as B1, B2, B3, …, B15. Notably, B5 is a needle roller bearing located within the planetary gear assembly, with a total of three such bearings. And B6 serves analogous functions within the system.

The planetary gear transmission system contains 10 gears. G1 is the sun gear of the first planetary stage, G2 is the planetary gear of the first stage, and G3 is the inner ring gear of the first planetary stage. G4, G5, and G6 represent the sun gear, planetary gear, and ring gear, respectively, of the second planetary stage. The motor's power is initially transmitted from shaft S1 to the sun gear G1 of the first planetary stage, which then drives the planetary carrier C1 through the planetary gears. Carrier C1 is coupled to the sun gear of the second planetary stage, and after passing through the second planetary stage, the power is transferred to the planetary carrier C2. Carrier C2 is connected to shaft S2, and the power on S2 is transmitted to S3 through the meshing of G7 and G8. Finally, the power is transmitted to S4 via the meshing of G9 and G10.

2.2. *Time-varying excitation forces analysis*

In addition to the dynamic behaviors that can be directly observed in experiment, such as rotational speed and vibration, the system exhibits several important nonlinear dynamic characteristics. Some of these responses are caused by internal time-varying excitation forces. One of the key excitations in is the TVMS. It is sensitive to changes in the gear surface, such as damage or other external factors, which can alter its behavior. Figure 4 illustrates the TVMS for various gear pairs in the drivetrain system. It is evident that the TVMS for all gear pairs is highly periodic, suggesting that the meshing conditions for all gears in the model remain relatively stable and optimal in the dynamic model. When comparing the TVMS between gear pairs G1–G2 and G2–G3, it is observed that the meshing time for double-tooth engagement between the planetary gear and the ring gear is significantly longer than the single-tooth meshing time between the planetary gear and the sun gear. This difference can be attributed to the higher contact ratio of meshing between the ring gear and the spur gear. Furthermore, it can be seen that the TVMS during the interaction between the planetary gear and the ring gear is

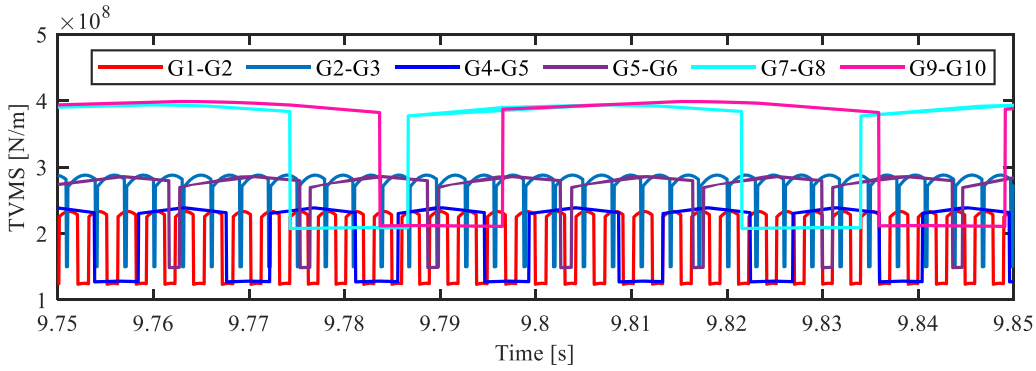


Figure 4. The TVMS of the gear pairs within the drivetrain system.

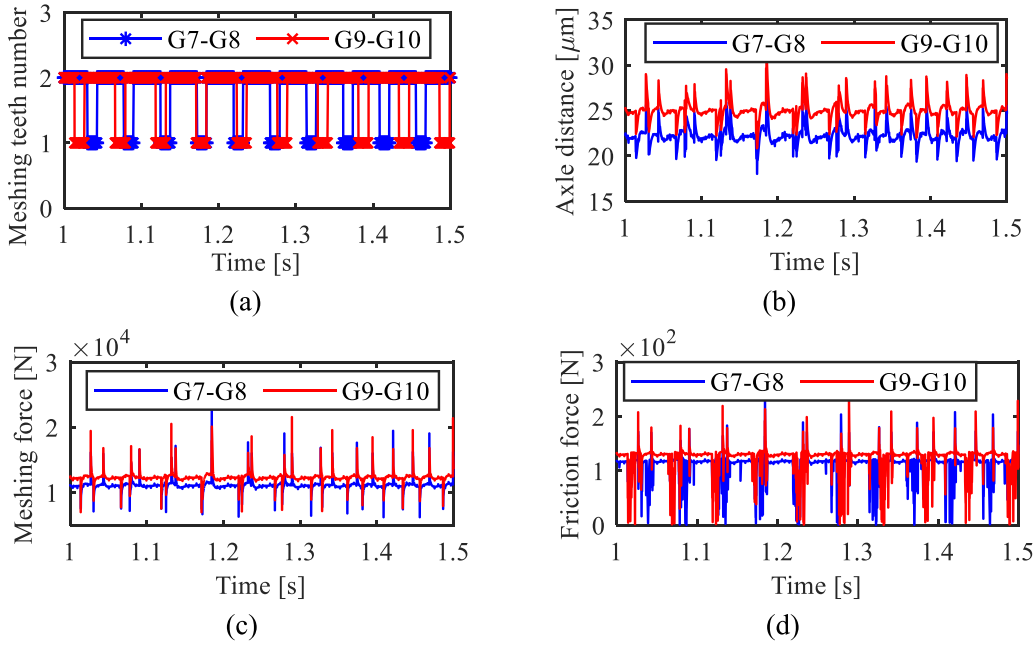


Figure 5. Time-varying dynamic characteristics of G7/G8 and G9/G10 that are difficult to test. (a) Meshing teeth number. (b) Axle distance. (c) Meshing force. (d) Friction force.

greater than that between the planetary gear and the sun gear. However, within the same planetary gear set, the meshing frequency between the planetary gear and the ring gear aligns with that between the planetary gear and the sun gear, as confirmed by comparing the TVMS of the G1–G2 and G2–G3 pairs. Additionally, the TVMS of gears G7 and G8, as well as G9 and G10, is slightly higher than that of the planetary gears, with a longer cycle duration. This suggests a reduction in rotational speed during the transmission process.

When spur gears mesh, they alternate between single-tooth and double-tooth engagements. However, it is challenging to experimentally determine the exact moments when the gears transition between these two meshing states. Figure 5(a) illustrates the time-varying meshing teeth number for the G7–G8 and G9–G10 gear pairs. Throughout the meshing process, the interaction of the meshing forces inevitably causes slight variations in the center distance between the gears. Figure 5(b) shows the time-varying center distance of the two spur gear pairs, while figure 5(c) presents the corresponding time-varying meshing forces. Additionally, when the gear surfaces experience contact compression, frictional forces are generated, as shown in figure 5(d), which depicts the time-varying frictional force for the two gear pairs. It is evident that these dynamic characteristics exhibit a certain periodicity, which is closely related to the meshing frequency of the gears. This periodic behavior reflects the underlying dynamics of gear meshing and provides insights into the interaction of forces within the system.

During the operation of a gear transmission system, the forces experienced by the bearings on the same shaft can vary, yet these forces are not easily measurable through direct sensor readings. Figure 6 illustrates the time-varying support forces acting on the four bearings of shaft S1. Understanding these forces is essential for accurately adjusting the bearing support positions and ensuring optimal system performance.

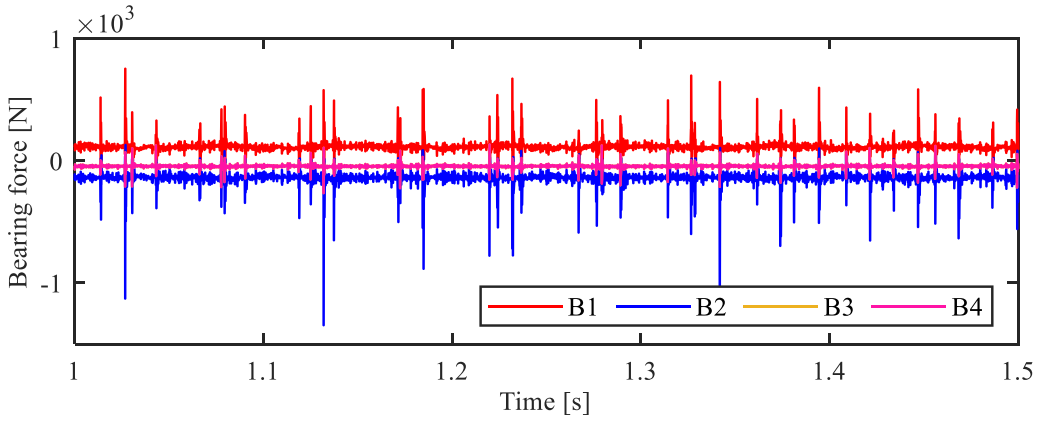


Figure 6. The bearing force of B1, B2, B3, and B4.

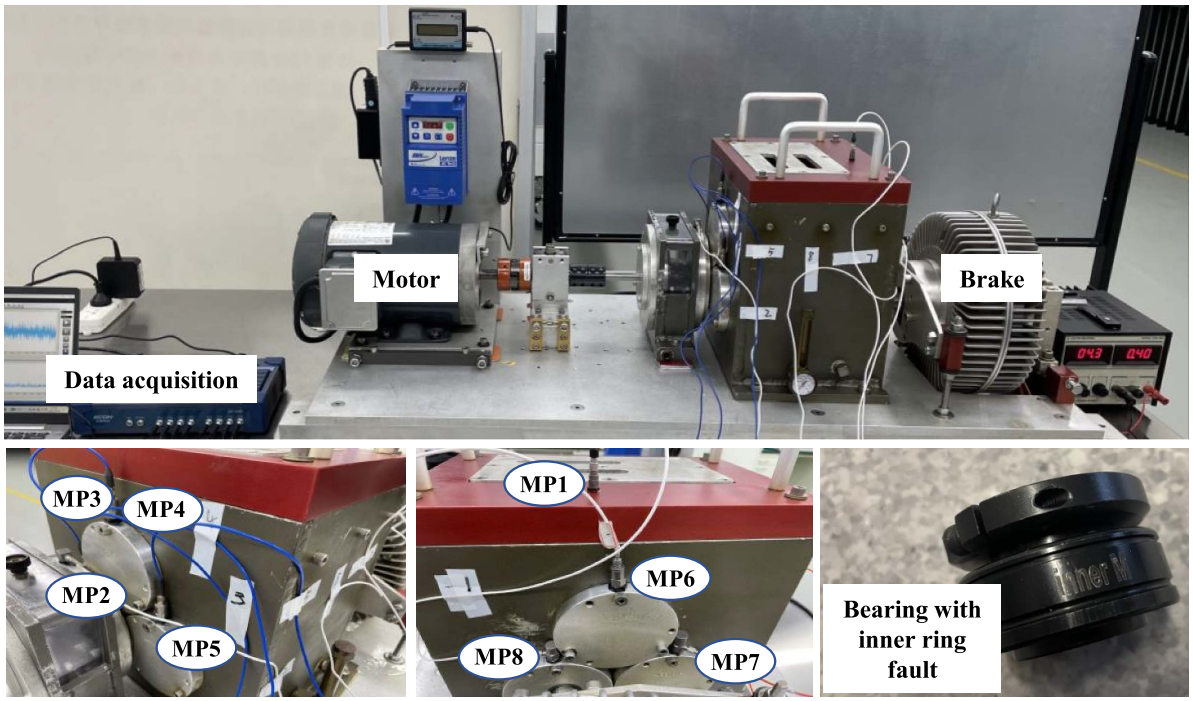


Figure 7. The planetary gearbox test bench and positions of vibration sensors.

3. Experimental verification

3.1. Introduction to the test bench

Figure 7 shows the physical object of the planetary gearbox test bench and the position of the vibration sensor. The planetary gearbox is driven by a three-phase asynchronous motor with 3 horsepower, and the load is applied by an eddy current brake. During the operation of the test bench, a load of 20 Nm was applied. To verify the correctness of the established model, we tested the vibration signals of the planetary gearbox under both healthy and B11 inner ring fault conditions. Different sensor signals are transmitted to the computer through a data acquisition device. Among the eight vibration sensors, MP1 is installed on the housing of the parallel shaft gear, MP2 is installed on the housing of the planetary gear, and MP3, MP4, MP5, MP6, MP7, and MP8 are measuring points on the six bearing seats of the parallel shaft, respectively.

3.2. Comparison of experimental and simulated signals

In a gear transmission system, the rotation of the shafts and the meshing of the gears induce significant vibrations within the gearbox. The input rotational speed of the test rig motor can be directly read from the tachometer, while the input rotational speed of the planetary gearbox simulation model will be set according to the experimental values. The rotational frequency is calculated as $f_r = r_{in}/60$, here r_{in} is the rotation speed of the rotating shaft and its unit is r min^{-1}. The meshing frequency is calculated as $f_m = z_g \cdot r_g/60$, here r_g is the rotation speed of the rotating gear and its unit is r min^{-1}, z_g refers to the number of

Table 1. Typical characteristic frequencies of drivetrain system.

Excitation frequencies		Symbols	Values (Hz)
The rotation frequencies of shafts	S1	f_{r1}	20
	S2	f_{r2}	4.374
	S3	f_{r3}	1.268
	S4	f_{r4}	3.172
The meshing frequencies of gear pairs	G1, G2, and G3	f_{m1}	——
	G4, G5, and G6	f_{m2}	437.4
	G7/G8	f_{m3}	126.8
	G9/G10	f_{m4}	114.12
Fault frequency	B11	f_o	6.882

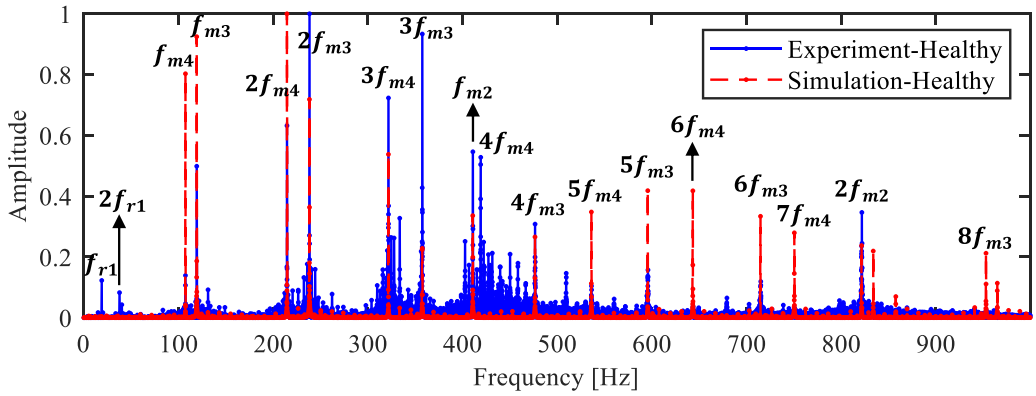


Figure 8. The comparison of experimental and simulated signals in healthy state.

teeth. Given the complex nature of the vibration signals in the planetary gear transmission system, the first-stage planetary gear set, comprising gears G1, G2, and G3, will be excluded in the subsequent vibration tests and simulations. In this modified configuration, the motor will directly transmit power to the sun gear G5 of the second-stage planetary gear set via the shaft S1. Both the simulation model of the planetary gearbox and the test bench have an input speed of 1200 r min^{-1}. Table 1 provides theoretical values of the primary rotational and meshing frequencies observed in the drivetrain system.

The vibration signals of different measuring points in healthy state are very similar, so here we take measuring point 6, which is closest to the faulty bearing, as an example to compare the test signals and simulation signals under healthy and faulty conditions. Figure 8 presents a comparison between the experimental vibration signals and the simulated signals. Both the simulated and experimental signals exhibit similar trends, with the meshing characteristic frequencies of the two pairs of spur gears being more prominent than the meshing frequency of the planetary gears. Notably, the maximum amplitude for these spur gear meshing frequencies occurs at twice the meshing frequency. Additionally, the rotational frequency of the power input shaft is clearly discernible in the experimental signal, but is relatively weak in the simulated signal. The rotational frequencies of the other shafts are less pronounced in both signals. In order to further quantify the difference between the simulation data and the experimental data, we calculated the Root Mean Square Error (RMSE) for two sets of normalized frequency domain data. The formula for RMSE is given by equation (6), here s_i represents the discrete points of the simulation data, e_i represents the discrete points of the experimental data. Both the experimental and simulation data consist of n discrete data points. After calculation, RMSE = 0.0283, which shows that the simulation data is very close to the experimental data

$$\mathrm{RMSE} = \sqrt{\frac{1}{n}\sum_{i=1}^{n}(s_i - e_i)^2}. \tag{6}$$

For the faulty state, using the inner ring fault of bearing B11 as an example, it is assumed that once the fault is implanted, the defective component will not undergo further degradation. Accordingly, in the digital twin model, the fault excitation introduced is a periodic excitation with a fixed period and amplitude, described by $F_{\mathrm{fault}} = A(t)\left[\sin(\pi f_o t)\right]^d$, where $A(t)$ is a constant, set to 50 N here. Furthermore, due to the fixed connection between the bearing's inner ring and the rotating shaft, and the simplification of the bearing into a stiffness-damping matrix during the modeling process, this periodic impact force can be treated as a periodic excitation acting on the rotating shaft. The corresponding value of f_o is provided in table 1 and $d = 1024$. The comparison of experimental and simulated signals with bearing fault is shown in figure 9.

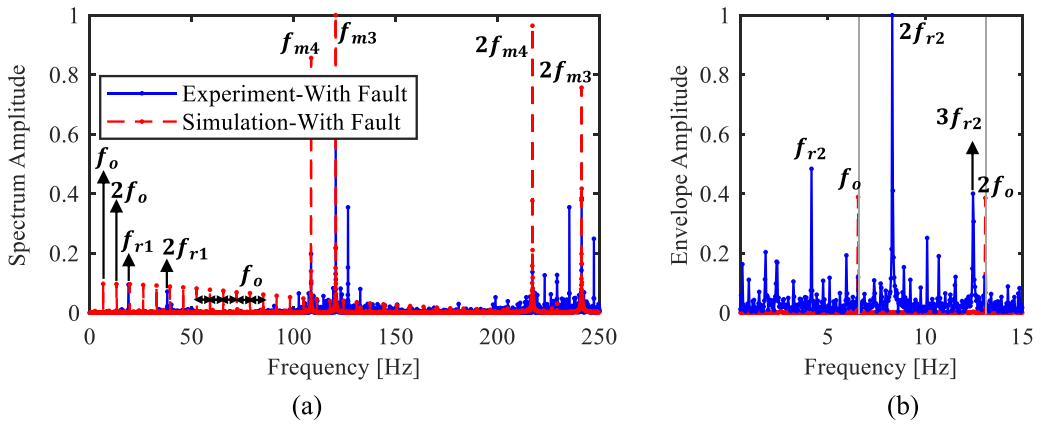


Figure 9. The comparison of experimental and simulated signals with bearing fault. (a) Spectrum. (b) Envelope spectrum.

Figure 9(a) presents a comparison of the spectra, while figure 9(b) displays the comparison of the envelope spectra. It is evident that the rotation and meshing frequencies are largely consistent with those of a healthy planetary gearbox. The key distinction lies in the fault characteristics, which are notably weak in the experimental data. In the envelope spectrum, only very faint harmonics at f_o and $2f_o$ can be detected, with their amplitudes significantly smaller than the rotation frequency of S1. This indicates that the bearing fault is minor, with its impact on the system being less pronounced than the influence of S1's rotational on the planetary gearbox. In contrast, the simulation data clearly reveal the fault characteristic frequencies. Similarly, we also quantified the difference between the experimental and simulation data under fault conditions, resulting in RMSE = 0.0293, which is bigger than that of healthy state. It can be observed that the difference between the simulation and experimental signals under fault conditions is larger than that under healthy conditions, primarily reflected in the fault signals. This is because the real experimental system is influenced by factors such as lubrication, making it difficult to detect early fault information. Additionally, when the fault information is transmitted from the bearing to the gearbox surface, significant attenuation occurs. In the simulation process, we have considered fewer factors related to signal attenuation, which results in the fault information being much more pronounced in the simulation. This illustrates the difficulty of accurately replicating physical systems using dynamic models. Nonetheless, it underscores the importance of using models to gain a deeper understanding of the dynamic behavior of physical systems and, ultimately, to derive the degradation patterns of such systems.

4. Degradation analysis based on dynamics simulation

Obtaining the degradation law of planetary gearboxes through fatigue testing is both time-consuming and costly. Therefore, leveraging the dynamic model of the planetary gear transmission system, we will perform a state degradation analysis of the planetary gearbox, using the inner ring damage progression of bearing B11 as a case study. Figure 10 illustrates the positions of the 8 measurement points in the dynamic model simulation data collected during the degradation analysis of the planetary gearbox. MP1 and MP2 locates on the housing and MP3, MP4, MP5, MP6, MP7, and MP8 locates on different bearing seats in the actual test system. The sensors placed on the bearing seat are specifically designed to capture vibration signals from within the planetary gearbox, thereby providing a more comprehensive reflection of the gearbox's degradation.

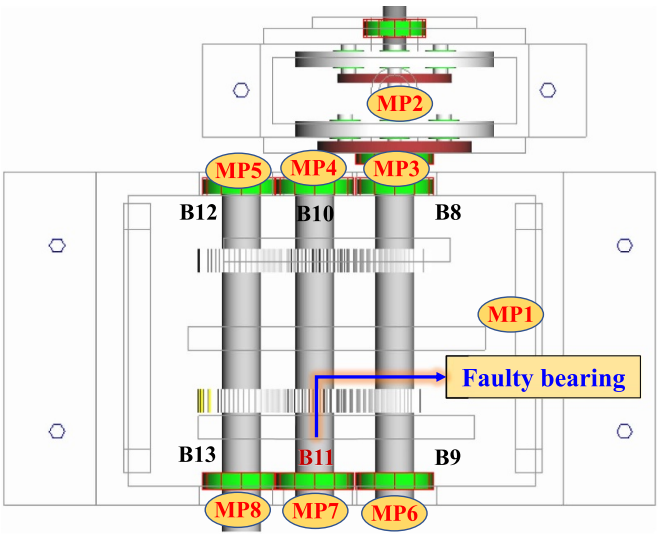


Figure 10. The positions of sensors on drivetrain system.

4.1. Bearing fault implantation and dynamic simulation

4.1.1. Excitation force for bearing fault. Bearings are critical components in planetary gearboxes, primarily serving to support the shaft. The degradation of planetary gearboxes is often manifested in the progressive damage to these key components. This paper examines the degradation process of planetary gearboxes, using the expansion of damage to the bearing inner ring as a case study. As illustrated in figure 11(a), when a defect occurs in the inner ring of the bearing, each roller

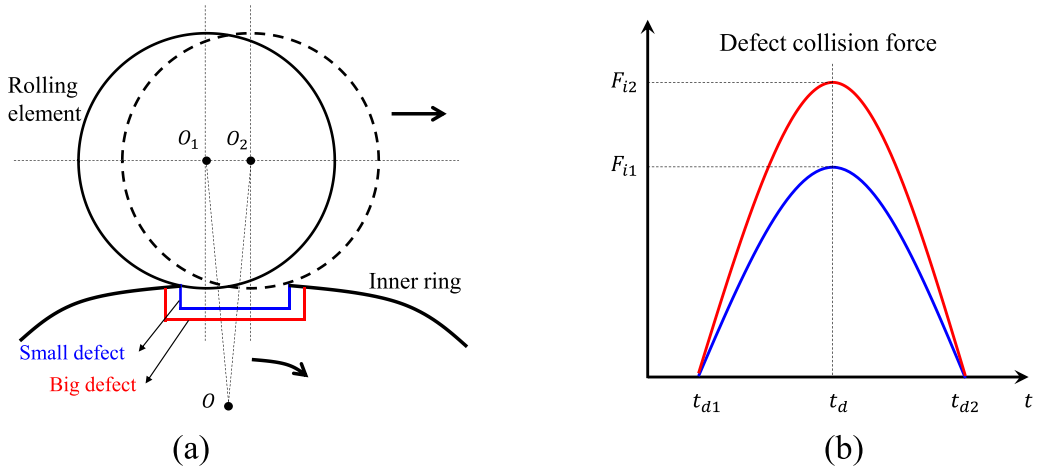


Figure 11. Bearing inner ring defect and impact force. (a) Kinematic relationships of rolling bearing. (b) Fault excitation forces corresponding to different defect sizes.

passing through the defective area generates an impact. In this study, we represent the defects in the bearing inner ring as a periodic impact force, as shown in figure 11(b). As the defect grows from a small to a larger size, the amplitude of the impact force increases, transitioning from F_{i1} to F_{i2}. Furthermore, due to the fixed connection between the bearing's inner ring and the rotating shaft this periodic impact force can be treated as a periodic excitation acting on the rotating shaft.

Here, a semi sine function is used to simulate the fault impact force $F_{\mathrm{fault}}(t)$, and its expression is shown in equation (7). Among them, $A(t)$ is the amplitude of the fault force, which gradually increases over time, indicating the damage propagation process of the bearing. d is a constant used to control the duration of an impact force. The larger d, the shorter the time from t_1 to t_2, but it does not affect the amplitude of the fault force. The calculation method for the frequency f_{o} of fault impact is shown in equation (8), where z is the number of rolling elements, f_{r} is the rotational frequency of the shaft, d_{B} is the diameter of the rolling elements, and D is the diameter of the bearing element, α is the contact angle

$$F_{\mathrm{fault}}(t) = A(t)\left[\sin\left(\pi f_{\mathrm{o}} t\right)\right]^{d} \tag{7}$$

$$f_{\mathrm{o}} = 0.5 z f_{\mathrm{r}}\left(1 + \frac{d_{\mathrm{B}}}{D}\cos\alpha\right). \tag{8}$$

When the bearing experiences damage, the affected area progressively expands due to repeated collisions. Consequently, it is assumed in this study that the fault excitation increases monotonically over time. Generally, when a bearing first experiences damage, the rate of damage propagation is slow. However, at a certain point in time, the damaged area can expand rapidly. This evolution process aligns with the characteristics of a power-law function, as shown in equation (9). And equation (10) presents the expression of fault excitation force whose amplitude changes with time following a power function law. The coefficients a and b of the power function are determined using the curve fitting toolbox in MATLAB, and c is set to 10 to ensure that the fitting function has a non-negative value. In this section, we will simulate the damage propagation process of B11 bearing, so the presented bearing fault excitation $F_{\mathrm{fault1}}(t)$ will act on S2 of the planetary gearbox. After incorporating this fault force into the planetary gearbox, we obtain the dynamic model of the planetary gearbox with bearing degradation. Here, we use the 100 s at the initial bearing degradation as an example to explain the process of developing the fault excitation force. This time period is sufficient to analyze the vibration characteristics of the planetary gearbox, and a longer simulation time would lead to a waste of computational resources. We assume that during the first 100 s of bearing degradation, the damage is relatively minor, and therefore, the applied fault excitation force does not need to be large. During the fitting process, 14 sets of discrete points are manually set. For the sake of simplicity, a 7 s interval is used, corresponding to the forces of 0, 10, 20, 50, 100, 200, 300, 400, 500, 600, 700, 800, 900, and 1000 N. Through the application of the least square's method, the discrete points are fitted to a power function, ultimately yielding the expression for the power function excitation force

$$A(t) = at^{b} + c \tag{9}$$

$$F_{\mathrm{fault1}}(t) = \left(at^{b} + c\right)\left(\sin\left(\pi f_{o} \mathrm{t}\right)\right)^{d}. \tag{10}$$

For $F_{\mathrm{fault1}}(t)$, $a = 0.2375$, $b = 1.829$, $c = 10$, and $d = 1024$.The excitation function for bearing faults can be represented by figure 12.

4.1.2. Vibration response analysis. Vibration velocity is known to provide a more accurate representation of the state of various frequency components across different frequency domains. Therefore, the vibration velocity at different measurement points on the planetary gearbox is utilized to monitor

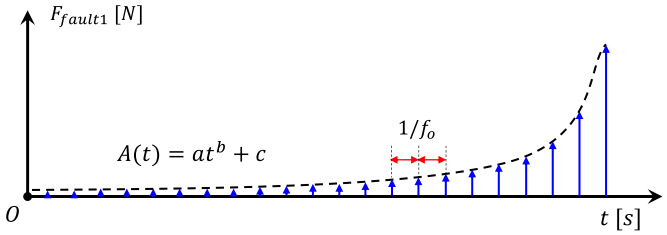


Figure 12. The time-varying bearing fault excitation.

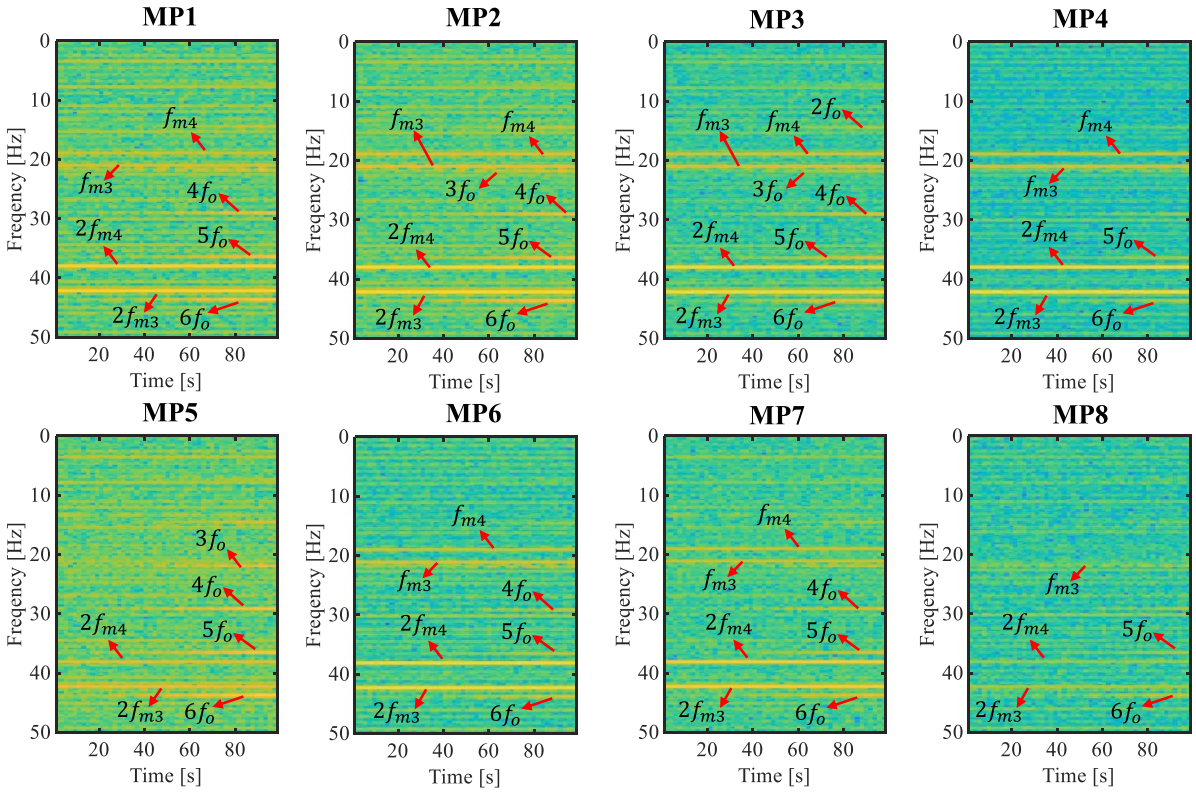


Figure 13. Time-frequency spectra of vibration signals with power function excitation.

the changes in vibration as the fault evolves. After incorporating the 100 s fault force into the dynamic model of the planetary gearbox, the vibration responses at different measurement points of the gearbox are simulated. Through the analysis of the simulation results, we find that it is difficult to extract the bearing fault characteristics using time-domain vibration signals. To investigate the changes in the vibration signals at each measurement point over time, we apply the Short-Time Fourier Transform (STFT) to the vibration signals in order to examine the degradation state of the planetary gearbox. Figure 13 illustrates the STFT spectra of the vibration signals at each measurement point under fault excitation.

From these spectra, it is evident that the meshing frequency of the two sets of spur gears, f_{m3} and f_{m4} remain present throughout the entire simulation. Over time, the fault characteristic frequency of the bearings becomes more pronounced. Notably, higher harmonics of the fault characteristic frequency emerge significantly earlier than the fundamental harmonic. For instance, in the M1 signal, the fault characteristic frequency f_o becomes detectable around 40 s and grows more distinct over time, while the sixth harmonic ($6f_o$) is observable from approximately 20 s. Similar trends are observed at other measurement points. Additionally, it is noteworthy that the fault characteristic frequencies at MP8 are less pronounced, likely due to the proximity of MP8 to the output end, where it is subjected to greater interference.

In order to clarify the process of vibration signals changing over time more clearly, we divided the vibration signal throughout the simulation process into 21 equally spaced signal segments. The vibration signals acquired at each interval can be expressed by equation (11), with the corresponding vibration level at each point determined by the numerical value obtained from equation (12). Here v_j represents the signal collected by the j_{th} sensor, and p represents the length of the signal. RMS_{vj} represents the vibration intensity of the planetary gearbox from the j_{th} measuring point at this interval. From

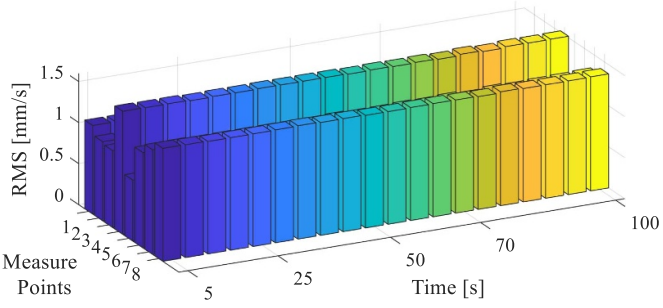


Figure 14. RMS values of vibration velocity values at different measure points.

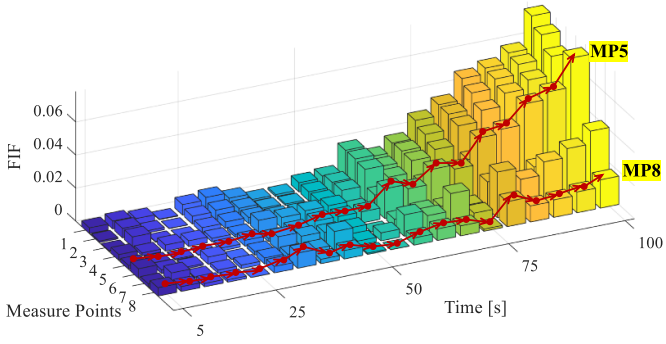


Figure 15. Changes in the FIF_{vj} at various measuring points under different fault forces.

figure 14, It is clear that the widely RMS value at each measurement point remained relatively stable over time, with no significant increase observed despite the introduction of fault force

$$\boldsymbol{v_j} = (v_{j1}, v_{j2}, \ldots, v_{jp}) \tag{11}$$

$$\mathrm{RMS}_{vj} = \sqrt{\sum_{i=1}^{p} v_{ji}^2}. \tag{12}$$

4.2. The new degradation indicator

From the existing literature and full-life degradation data, it is evident that the intensity of vibration signals can effectively monitor the health status of mechanical equipment. However, this may only be effective when the fault severity has evolved to a relatively significant level. To enable effective monitoring at the initial stages of fault occurrence within planetary gearboxes, this paper proposes a novel vibration intensity-based index FIF_{vj}. The mathematical expression for FIF_{vj} is provided in equation (13), where RMS_{vj} denotes the vibration intensity of the j_{th} sensor at each time interval after fault excitation is applied, and RMS_{vj0} represents the corresponding vibration intensity when no excitation force is applied

$$\mathrm{FIF}_{vj} = \left|\mathrm{RMS}_{vj} - \mathrm{RMS}_{vj0}\right|. \tag{13}$$

The FIF_{vj} values are calculated for each time period within 100 s, and the resulting data are presented in figure 15. It is evident that, over time, the fault impact at different measurement points tends to increase, suggesting that vibration information from various measurement points can effectively capture the degradation process of the planetary gearbox. Taking MP5 as an example, the vibration response of the planetary gearbox exhibits an overall upward trend, albeit with some irregular fluctuations and occasional decreases. This behavior is likely due to the inherent nonlinearity within the planetary gearbox. Furthermore, the sensitivity of different measurement points to bearing degradation information varies, with MP5 showing significantly higher sensitivity than MP8. Unlike the traditional RMS value of vibration signals presented in figure 14, the newly proposed indicator presented in figure 15 demonstrates a high sensitivity to fault information. It can effectively capture the evolution of bearing faults, which is of significant importance for characterizing the entire lifecycle degradation process of planetary gearboxes.

The performance degradation of planetary gearboxes can be effectively characterized by a unified indicator, enabling a more efficient assessment of their health condition. To achieve this, we aim to propose a comprehensive indicator that can integrate data from q different sensors, where $q = 8$. Based on the calculation methods of common time-domain metrics, table 2 presents 14 different degradation indicators as alternatives.

Furthermore, the vibration signal is divided into equal time intervals, and the indicators obtained for each interval reflect the degradation status of the planetary gearbox at that specific moment. The calculation results of each degradation indicator are shown in figure 16. Different indicators exhibit distinct characteristics. As shown on the left side of figure 16, the four indicators DI_{10}, DI_{11}, DI_{12}, and DI_{13} show a significant upward trend at the early stage of the fault. However, as the bearing fault evolves, they do not exhibit a notable change trend, making them unsuitable as degradation indicators. On the right side of figure 16, it is evident that most indicators show an upward trend as the severity of bearing damage increases. But different indicators demonstrate varying sensitivities to bearing faults. We can observe that DI_1 is the most sensitive to the evolution of bearing faults. In addition, the new degradation indicator is primarily based on vibration signals collected in the time domain. Compared to degradation indicators constructed using spectral structures, the calculation process of DI_1 is simpler and it is less sensitive to the effects of rotational frequencies or gear mesh frequencies in the planetary gearbox. Based on these advantages, it will be easily applied in the engineering.

Compared to degradation indicators, health indicators may be able to more intuitively reflect the health status of planetary gearboxes. Therefore, we propose a new normalized planetary gearbox health index $HI(t)$ based on the degradation index $DI_1(t)$. Its calculation method is shown in equation (14) and $DI_1(t)$ is the calculation result of DI_1 of the planetary gearbox

Table 2. Degradation indicators for comparison.

Number	Meaning	Expression	Number	Meaning	Expression
1	Root mean square	$DI_1 = \sqrt{\sum_{j=1}^{q} \mathrm{FIF}_{vj}^2}$	8	Kurtosis	$DI_8 = \frac{1}{q}\sum_{j=1}^{q} \mathrm{FIF}_{vj}{}^4$
2	Mean	$DI_2 = \frac{1}{q}\sum_{j=1}^{q} \mathrm{FIF}_{vj}$	9	Skewness	$DI_9 = \frac{1}{q}\sum_{j=1}^{q} \mathrm{FIF}_{vj}{}^3$
3	Peak to peak	$DI_3 = DI_4 - DI_5$	10	Margin indicator	$DI_{10} = DI_4/DI_7$
4	Maximum	$DI_4 = \mathrm{MAX}(\mathrm{FIF}_{v1}, \ldots, \mathrm{FIF}_{vq})$	11	Crest factor	$DI_{11} = DI_1/DI_2$
5	Minimum	$DI_5 = \mathrm{MIN}(\mathrm{FIF}_{v1}, \ldots, \mathrm{FIF}_{vq})$	12	Impulse factor	$DI_{12} = DI_4/DI_2$
6	Standard deviation	$DI_6 = \sqrt{\frac{1}{j-1}\sum_{j=1}^{q} \left[\mathrm{FIF}_{vj} - \overline{\mathrm{FIF}_{vj}}\right]^2}$	13	Peak factor	$DI_{13} = DI_4/DI_2$
7	Root square amplitude	$DI_7 = (\frac{1}{q}\sum_{j=1}^{q} \sqrt{\mathrm{FIF}_{vj}})^2$	14	Kurtosis factor	$DI_{14} = DI_8/DI_2{}^4$

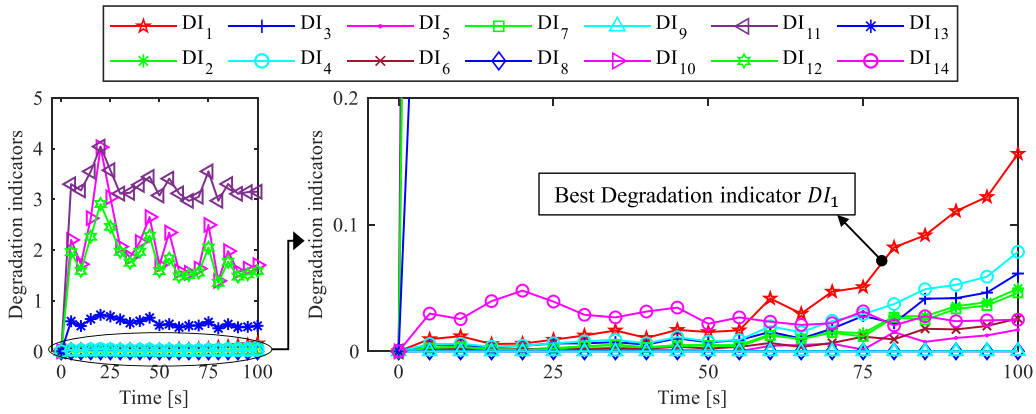


Figure 16. Degradation process of planetary gearbox under bearing fault excitation.

at each moment t, DI_1^{end} is the calculated result of DI_1 for the planetary gearbox when the bearing ultimately reaches damage. This new indicator will be used to characterize the full life degradation process of the bearing in the planetary gearbox

$$HI(t) = 100\% \times \left(1 - \frac{DI_1(t)}{DI_1^{\mathrm{end}}}\right). \tag{14}$$

4.3. Lifetime performance degradation analysis for the planetary gearbox

A time span of 100 s is too short relative to the full lifespan of the bearing. Therefore, we will next conduct full lifetime degradation simulation and analysis of the bearings in the planetary gearbox. In real engineering, it may take several years for a bearing to be completely damaged, but recording the complete cycle of twin data at all times requires a lot of time and calculation. Therefore, we adopt sparse sampling method to qualitatively study the degradation process of planetary gearboxes.

When a bearing deteriorates to the point where it is no longer functional, a significant increase in the vibration signal on the planetary gearbox is inevitably observed. Based on extensive life-cycle experimental data found in the literature [6], it has been established that upon bearing failure, the vibration signal amplitude increases by a factor of 5–10 compared to its initial value. In this context, we assume that when the vibration signal amplitude on the planetary gearbox surface reaches approximately five times the initial value, the bearing has reached the end of its service life. Through simulation experiments, it was determined that the corresponding fault excitation amplitude is around 20 000 N. Consequently, we model the fault excitation force amplitude as a power function, with the amplitude ranging from 0 to 20 000 N, while maintaining a constant excitation frequency. At the same time, we set this bearing to run for 8 h a day, 300 d a year, and finally reach the end of its life after 2400 h. By using the curve fitting toolbox in Matlab, we obtained the expression of the excitation force function as $F_{\mathrm{fault2}}(t) = \left(0.01367t^{1.829} + 10\right)\left(\sin\left(7.2913\pi t\right)\right)^{1024}$. By incorporating this simulated excitation force into the

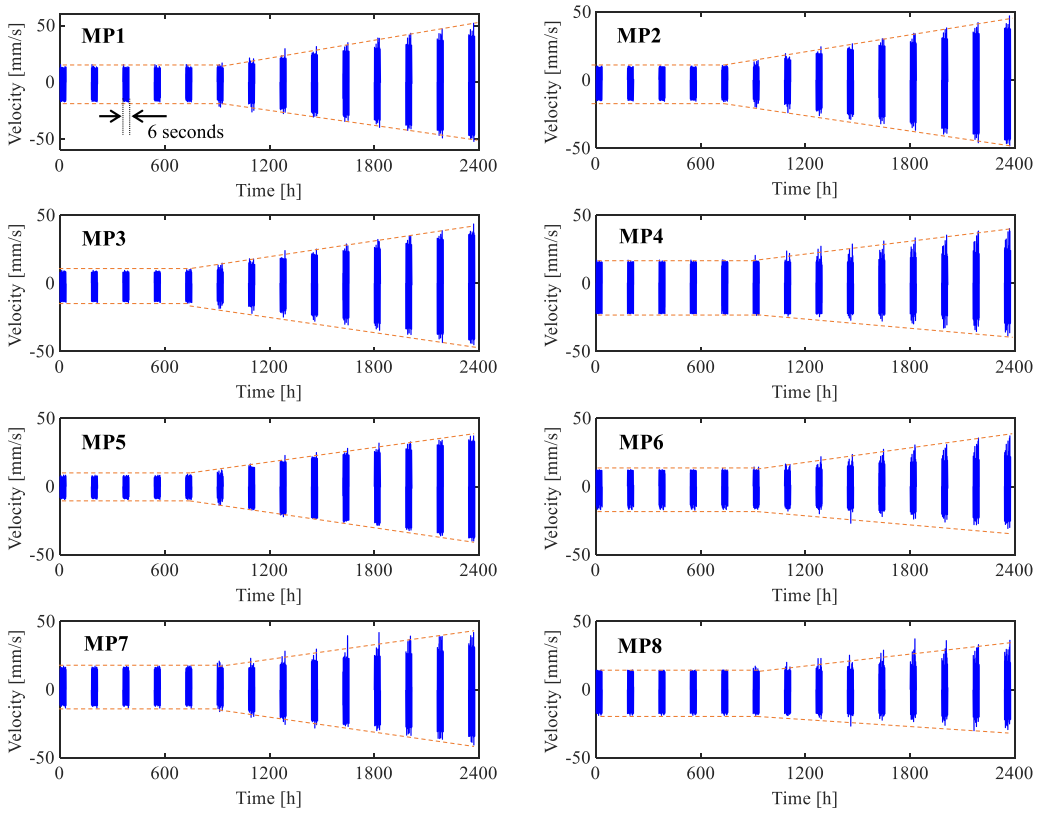


Figure 17. Twin vibration data of planetary gearbox degradation.

dynamic model of the planetary gearbox, we obtain a physics model of the entire lifecycle of the planetary gearbox. Figure 17 presents the twin data illustrating the degradation process of the planetary gearbox. Here 14 time points are selected across the entire lifecycle for analysis, with each point representing a data duration of 6 s. It is evident that, as time progresses, the vibration intensity of the planetary gearbox at various positions increases significantly, in contrast to the simulation results for a 100 s period, where vibration remains largely unchanged. However, the extent to which bearing degradation is perceived varies depending on the data obtained from different measurement points. MP5 consistently provides the most indicative degradation information, while MP8 exhibits a relatively slower response.

Due to the huge amount of data throughout the entire lifecycle, we are unable to obtain the changes in fault frequency characteristics in different measurement point signals during the degradation of planetary gearboxes through STFT. Therefore, we conducted spectral analysis on signals at different time points, and the results are shown in figure 18. We can intuitively obtain the evolution of the fault characteristic frequency of the bearing inner race over time throughout the entire lifecycle. It can be seen that as the bearings degrade, the peak values of fault characteristic frequency f_o and their harmonics $2f_o, 3f_o, 4f_o, 5f_o$ and $6f_o$ continue to rise. This indicates that the signals obtained from any of the eight measurement points can reflect the damage evolution process of the bearing in the planetary gearbox. However, the sensitivity to the degradation of the planetary gearbox varies across different measurement points. Interestingly, based on the upward trend of the fault frequency from the spectra, although MP7 is the closest measurement point to the faulty bearing, its sensitivity to fault degradation is not higher than that of MP2, which is the farthest from the fault location. This further demonstrates the limitations of relying solely on data from a single measurement point to monitor the degradation of the planetary gearbox. Therefore, it is crucial to perform a more in-depth analysis of the degradation state of the planetary gearbox based on the proposed new indicators, FIF and DI_1.

Figure 19(a) illustrates the state degradation process of the planetary gearbox, quantified using the proposed indicators FIF and DI_1. Figure 19(b) shows the time-varying health indicator values and the process of performance degradation. It is evident that MP1, MP2, and MP3 are highly sensitive to the degradation process. However, the advantages of these measurement points are not apparent in previous signal processing. Interestingly, MP5, which was previously identified as the most sensitive to bearing degradation during signal analysis, does not exhibit significant sensitivity in this case. This highlights the challenge of identifying an optimal measurement point that most effectively reflects the degradation process of the planetary gearbox. The degradation trend, represented by the comprehensive index DI_1, which integrates data from

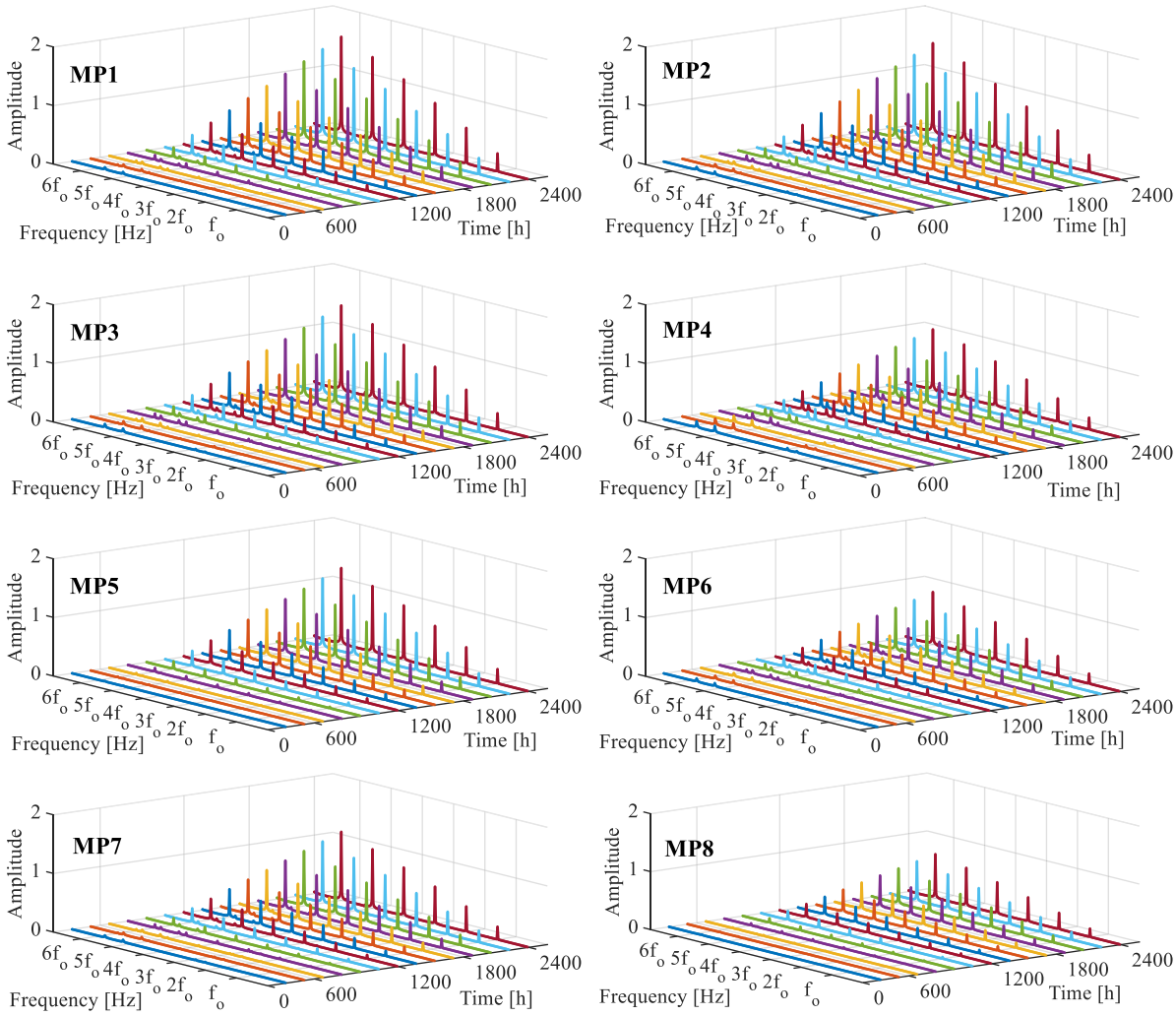


Figure 18. Spectrums of twin signals from different measurement points.

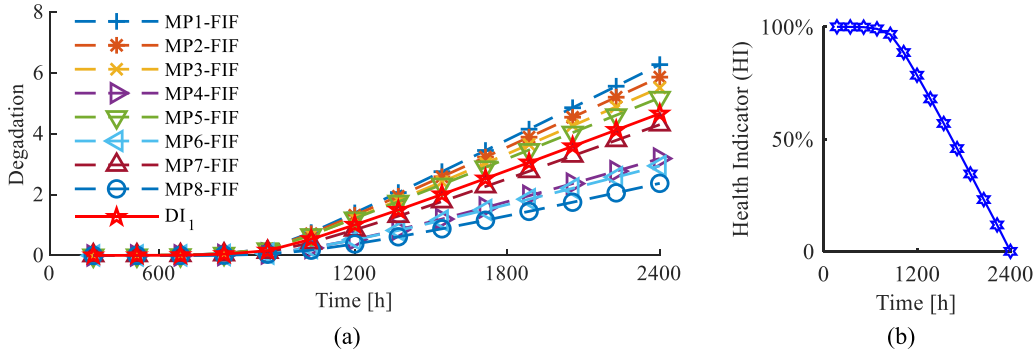


Figure 19. Characterization of full life degradation of the planetary gearbox bearing. (a) The degradation results of different measure points. (b) The time-varying health indicator values.

multiple sensors, is depicted by the red line. The HI (Health Indicator) derived from DI_1 provides a clear and intuitive representation of the degradation status of the planetary gearbox. In this way, the failure process of the bearing inner ring and the degradation of the planetary gearbox are quantitatively represented through the simulation results derived from the physical model.

5. Conclusions and future work

Experimental degradation data of planetary gearboxes is hard to obtain, challenging predictive maintenance. The primary innovation of this paper lies in the development of a dynamic model for planetary gearboxes that includes bearing fault excitation forces evolving over time, and the proposal of a

highly effective state degradation index, which can be used to perform an effective assessment of the full life cycle condition of the planetary gearbox based on physical simulation. The main contributions are as follows:

(1) A complex multi-body dynamic model of the gear transmission system, characterized by high complexity and comprehensive consideration of nonlinear factors has been established and experimentally validated. Simulations using this model analyzed dynamic characteristics difficult to measure experimentally, such as TVMS, DTE, time-varying meshing tooth count, and bearing support force.
(2) The expansion of the bearing inner race damage area is replaced by a periodic fault excitation force with an increasing amplitude over time and incorporated into the planetary gearbox dynamics model. Vibration signals from eight different measurement points were simulated, and the fault evolution characteristics were analyzed and visually presented.
(3) Based on the dynamic model of the planetary gearbox with degradation characteristics and simulation signals from various measurement points, a novel and effective degradation indicator was developed to capture the degradation behavior of the planetary gearbox. The lifetime performance degradation process of planetary gearbox has been clearly and intuitively characterized.

However, there is still room for further improvement in the accuracy of the simulation model and the robustness of the degradation analysis methods. In the future, we will investigate the following problems

(1) Refine the modeling approach by adopting a more accurate degradation excitation modeling method to enhance the precision of the simulation model.
(2) Introduce noise interference into the simulation results and compare them with degradation indicators based on experimental data from existing studies, further discussing the robustness of the method proposed.

References

[1] Liu J, Li X, Pang R and Xia M 2023 Dynamic modeling and vibration analysis of a flexible gear transmission system *Mech. Syst. Signal Process.* **197** 110367
[2] Pedrero J I, Sánchez-Espiga J, Sánchez M B, Pleguezuelos M, Fernández-del-rincón A and Viadero F 2024 Simulation and validation of the transmission error, meshing stiffness, and load sharing of planetary spur gear transmissions *Mech. Mach. Theory* **203** 105800
[3] Mo S, Wang Z, Tang X, Zhou Y, Zhang J and Zhang W 2024 Nonlinear dynamics of planetary gearboxes containing cracks *Nonlinear Dyn.* **112** 17007–31
[4] Chen X, Yang X, Zuo M J and Tian Z 2020 Dynamic modeling of a planetary gearbox with sun gear crack and bearing clearance *2020 Asia-Pacific Int. Symp. on Advanced Reliability and Maintenance Modeling (APARM)* pp 1–6
[5] Li H, Zhang Z, Li T and Si X 2024 A review on physics-informed data-driven remaining useful life prediction: challenges and opportunities *Mech. Syst. Signal Process.* **209** 111120
[6] Wang B, Lei Y, Li N and Li N 2020 A hybrid prognostics approach for estimating remaining useful life of rolling element bearings *IEEE Trans. Reliab.* **69** 401–12
[7] Qin Y, Wu X and Luo J 2022 Data-model combined driven digital twin of life-cycle rolling bearing *IEEE Trans. Ind. Inform.* **18** 1530–40
[8] Li X, Teng W, Zhang Y, Peng D and Liu Y 2025 Dynamic normalized health indicator construction and Bayesian recurrent state estimation for remaining useful life prediction of high-speed bearings in wind turbine drivetrain *Measurement* **246** 116725
[9] Ni Q, Ji J C and Feng K 2023 Data-driven prognostic scheme for bearings based on a novel health indicator and gated recurrent unit network *IEEE Trans. Ind. Inform.* **19** 1301–11
[10] Mao W, He J and Zuo M J 2020 Predicting remaining useful life of rolling bearings based on deep feature representation and transfer learning *IEEE Trans. Instrum. Meas.* **69** 1594–608
[11] Zhu J, Chen N and Shen C 2020 A new data-driven transferable remaining useful life prediction approach for bearing under different working conditions *Mech. Syst. Signal Process.* **139** 106602
[12] Deng Y, Du S, Wang D, Shao Y and Huang D 2023 A calibration-based hybrid transfer learning framework for RUL prediction of rolling bearing across different machines *IEEE Trans. Instrum. Meas.* **72** 1–15
[13] Ma Z *et al* 2025 Two novel indicators for gear crack diagnosis based on vibration responses: experiment and simulation *Mech. Mach. Theory* **205** 105905
[14] Ni X, Zhao J, Hu Q, Zhang X and Li H 2017 A new improved Kurtogram and its application to planetary gearbox degradation feature analysis *J. Vibroeng.* **19** 3413–28
[15] Pan Y, Hong R, Chen J, Singh J and Jia X 2019 Performance degradation assessment of a wind turbine gearbox based on multi-sensor data fusion *Mech. Mach. Theory* **137** 509–26
[16] Sun D, Wang B, Hu X and Wang W 2019 An online degradation feature extraction technique for shore bridge gearbox based on morphological fractal dimension and sliding window Weibull fitting *Shock Vib.* **2019** 9216809
[17] Ma Y, Jia X and Bai H 2020 Gearbox degradation assessment based on a sparse representation feature and Euclidean distance technique *Aust. J. Mech. Eng.* **20** 500–15
[18] Qiao W, Ni X, Wang L, Lv X, Chen L and Sun F 2021 New degradation feature extraction method of planetary gearbox based on alpha stable distribution *J. Mech. Sci. Technol.* **35** 1–19
[19] Chen X, Wang Y, Sun H, Ruan H, Qin Y and Tang B 2023 A generalized degradation tendency tracking strategy for gearbox remaining useful life prediction *Measurement* **206** 112313
[20] Caso E, Fernandez-Del-Rincon A, Garcia P, Diez-Ibarbia A and Sanchez-Espiga J 2023 An experimental study of acoustic emissions from active surface degradation in planetary gears *Mech. Syst. Signal Process.* **189** 110090
[21] Luo M, Guo Y, Su Z, André H, Tang Z, Zhou C and Li C 2025 Defect quantification evaluation of a rolling element bearing based on physical modelling and instantaneous vibration energy investigation *J. Sound Vib.* **600** 118875
[22] Shi H, Song Z, Bai X, Hu Y, Li T and Zhang K 2023 A novel digital twin model for dynamical updating and real-time mapping of local defect extension in rolling bearings *Mech. Syst. Signal Process.* **193** 110255
[23] Ma L, Jiang B, Xiao L and Lu N 2023 Digital twin-assisted enhanced meta-transfer learning for rolling bearing fault diagnosis *Mech. Syst. Signal Process.* **200** 110490
[24] Song W, Guo L, Yu Y, Gao H, Xu H and Feng T 2025 A parameter-interactive digital twin model of

bearings under variable speeds *Measurement* **244** 116307
[25] Zhao W, Zhang C, Fan B, Wang J, Gu F, García Peyrano O, Wang S and Lv D 2023 Research on rolling bearing virtual-real fusion life prediction with digital twin *Mech. Syst. Signal Process.* **198** 110434
[26] Liu J, Cao H, Su S and Chen X 2023 Simulation-driven subdomain adaptation network for bearing fault diagnosis with missing samples *Eng. Appl. Artif. Intell.* **123** 106201
[27] Chen G, Tang Q, Li H and Sun K 2025 Rigid-flexible coupling dynamic-assisted imbalanced fault diagnosis for helicopter tail transmission system *Measurement* **242** 115934
[28] Ishihara T, Wang S and Kikuchi Y 2025 Fatigue prediction of wind turbine main bearing based on field measurement and three-dimensional elastic drivetrain model *Eng. Fail. Anal.* **167** 108985
[29] Zhu D, Li Z and Hu N 2022 Multi-body dynamics modeling and analysis of planetary gearbox combination failure based on digital twin *Appl. Sci.* **12** 12290
[30] Yang Y, Hu N, Li Y, Cheng Z and Shen G 2024 Dynamic modeling and analysis of planetary gear system for tooth fault diagnosis *Mech. Syst. Signal Process.* **207** 110946
[31] Wei C, Cao H, Shi J, Yang Y and Du M 2024 A novel method for vibration signal transmission and attenuation analysis in complex planetary gearboxes *Sci. China Technol. Sci.* **67** 2939–53
[32] Moghadam F K and Nejad A R 2022 Online condition monitoring of floating wind turbines drivetrain by means of digital twin *Mech. Syst. Signal Process.* **162** 108087
[33] Yu J, Wang S, Wang L and Sun Y 2023 Gearbox fault diagnosis based on a fusion model of virtual physical model and data-driven method *Mech. Syst. Signal Process.* **188** 109980
[34] Deng H, Kong J, Liu J, Hu Z, Sun Y, Guo Y, Song L and Yu H 2025 Fatigue reliability analysis methodology based on fatigue life and failure mechanism for carburized gear *Eng. Fail. Anal.* **167** 108950
[35] Feng K, Ji J C, Zhang Y, Ni Q, Liu Z and Beer M 2023 Digital twin-driven intelligent assessment of gear surface degradation *Mech. Syst. Signal Process.* **186** 109896
[36] Kumar R, Mandal S, Bhardwaj P, Mishra C and Mahato S 2025 Defect diagnosis of high contact ratio spur gear system with increasing level of fault *Eng. Fail. Anal.* **169** 109097
[37] Eichberger A and Hofmann G 2007 TMPT: multi-body package SIMPACK *Veh. Syst. Dyn.* **45** 207–16



Hongrui Cao obtained his PhD degree from Xi'an Jiaotong University in 2010. He is currently a professor at the School of Mechanical Engineering, Xi'an Jiaotong University. His research focuses primarily on digital twin modeling of major equipment, fault mechanism analysis, fault diagnosis. He has published more than 100 SCI/EI papers, four of which have been selected as ESI Highly Cited Papers. Since 2019, he has been continuously ranked among the top 2% of scientists worldwide and has been included in Elsevier's 'Highly Cited Chinese Researchers' list.



Chaohu Wei obtained his bachelor's degree from Jilin University in 2020. He is currently pursuing his PhD at the School of Mechanical Engineering, Xi'an Jiaotong University. His research focuses primarily on digital twin modeling of complex gear transmission systems, fault mechanism analysis, and vibration testing. In 2024, he was awarded the National Scholarship for Doctoral Students by the Ministry of Education of the People's Republic of China.



Xuefeng Chen obtained his PhD degree from Xi'an Jiaotong University in 2004. He is currently a professor at the School of Mechanical Engineering, Xi'an Jiaotong University. His research focuses primarily on intelligent detection of major mechanical equipment, fault diagnosis and intelligent operation and maintenance. He has won numerous prestigious awards, including the National Technology Invention Award of the People's Republic of China and the Natural Science Award from the Ministry of Education. The mechanical equipment health management and intelligent diagnostic system he developed has been deployed in tens of thousands of units.